

Generating two-dimensional quantum gases with high stability

Bo Xiao(肖波), Xuan-Kai Wang(王宣恺), Yong-Guang Zheng(郑永光), Yu-Meng Yang(杨雨萌), Wei-Yong Zhang(章维勇), Guo-Xian Su(苏国贤), Meng-Da Li(李梦达), Xiao Jiang(江晓), Zhen-Sheng Yuan(苑震生)

Citation: Chin. Phys. B . 2020, 29(7): 076701 . **doi:** 10.1088/1674-1056/ab8ac8
Journal homepage: http://cpb.iphy.ac.cn; http://iopscience.iop.org/cpb

What follows is a list of articles you may be interested in

Accelerate Bose-Einstein condensate by interaction

Jie-Li Qin(秦杰利)

Chin. Phys. B . 2019, 28(12): 126701 . **doi:** 10.1088/1674-1056/ab4e8a

Propagation of dark soliton interacting with domain wall in two immiscible Bose-Einstein condensates

Lang Zheng(郑浪), Yi-Cai Zhang(张义财), Chao-Fei Liu(刘超飞)

Chin. Phys. B . 2019, 28(11): 116701 . **doi:** 10.1088/1674-1056/ab457e

Expansion dynamics of a spherical Bose-Einstein condensate

Rui-Zong Li(李睿宗), Tian-You Gao(高天佑), Dong-Fang Zhang(张东方), Shi-Guo Peng(彭世国), Ling-Ran Kong(孔令冉), Xing Shen(沈星), Kai-Jun Jiang(江开军)

Chin. Phys. B . 2019, 28(10): 106701 . **doi:** 10.1088/1674-1056/ab4177

Bloch oscillation of Weyl metal along synthetic dimensions

Ye Xiong(熊烨)

Chin. Phys. B . 2018, 27(12): 126701 . **doi:** 10.1088/1674-1056/27/12/126701

A combined system for generating a uniform magnetic field and its application in the investigation of Efimov physics

Rui Yao(姚睿), Zhen-Dong Sun(孙震东), Shu-Yu Zhou(周蜀渝), Ying Wang(王颖), Yu-Zhu Wang(王育竹)

Chin. Phys. B . 2018, 27(1): 016703 . **doi:** 10.1088/1674-1056/27/1/016703

Generating two-dimensional quantum gases with high stability*

Bo Xiao(肖波)[1,2], Xuan-Kai Wang(王宣恺)[1,2], Yong-Guang Zheng(郑永光)[1,2], Yu-Meng Yang(杨雨萌)[1,2], Wei-Yong Zhang(章维勇)[1,2], Guo-Xian Su(苏国贤)[1,2], Meng-Da Li(李梦达)[1,2], Xiao Jiang(江晓)[1,2], and Zhen-Sheng Yuan(苑震生)[1,2,†]

[1] *Hefei National Laboratory for Physical Sciences at the Microscale, and Department of Modern Physics, University of Science and Technology of China, Hefei* 230026, *China*

[2] *CAS Center for Excellence in Quantum Information and Quantum Physics, Hefei* 230026, *China*

(Received 14 February 2020; revised manuscript received 13 April 2020; accepted manuscript online 20 April 2020)

Quantum gas microscopy has enabled the study on intriguing properties of ultracold atoms in optical lattices. It provides the cutting-edge technology for manipulating quantum many-body systems. In such experiments, atoms have to be prepared into a two-dimensional (2D) system for being resolved by microscopes with limited depth of focus. Here we report an experiment on slicing a single layer of the atoms trapped in a few layers of pancake-shaped optical traps to create a 2D system. This technique is implemented with a microwave "knife", i.e., a microwave field with a frequency defined by the resonant condition with the Zeeman-shifted atomic levels related to a gradient magnetic field. It is crucial to keep a stable preparation of the desired layer to create the 2D quantum gas for future experimental applications. To achieve this, the most important point is to provide a gradient magnetic field with low noises and slow drift in combination with a properly optimized microwave pulse. Monitoring the electric current source and the environmental magnetic field, we applied an actively stabilizing circuit and realized a field drift of 0.042(3) mG/hour. This guarantees creating the single layer of atoms with an efficiency of 99.92(3)% while atoms are hardly seen in other layers within 48 hours, satisfying future experimental demands on studying quantum many-body physics.

Keywords: ultracold atoms, optical lattices, two-dimensional quantum gases, quantum-gas microscope

PACS: 67.85.–d, 05.30.–d, 37.10.Jk **DOI:** 10.1088/1674-1056/ab8ac8

1. Introduction

Ultracold atoms in optical lattices have been demonstrated to be very promising for studying quantum many-body physics.[1] In particular, quantum gas microscopy (QGM), composed of optical lattices and high-resolution imaging approaches, has becoming a cutting edge method for studying quantum crystals in a brand-new way.[2–7] Experiments such as measurement of Rényi entropy of a few-body system,[8] and *in situ* observation of many-body localization[9] have been performed with QGM, making it a unique tool for quantum simulation with ultracold atoms.

In three-dimensional (3D) lattices, it is of challenge to distinguish atoms in neighboring layers due to the fact that the depth of focus of the microscope is usually larger than the lattice constant. Moreover, the fluorescence emitted by out-of-focus atoms will blur the signal arising from the in-focus plane, damaging the imaging contrast. Therefore, it is important to prepare atoms in a monolayer for further studies. Furthermore, the 2D system is of great research interest for observing various quantum phenomena such as the Berezinsky–Kosterlitz–Thouless (BKT) transition.[10,11]

In principle, there are two different approaches to prepare 2D quantum gases. One is to compress a three-dimensional cloud of ultracold atoms with light sheets and load them into one layer of a one-dimensional (1D) optical lattices,[7,12] or into a surface trap.[13,14] The other approach, as demonstrated herein, starts with an 1D optical lattice consisting parallel pancake-like traps filled with atoms. Then a microwave "knife" is used to flip the internal state of one layer of the Zeeman-shifted atoms in the presence of a gradient magnetic field. The rest atoms which are not selected will be blown away from the system by a resonant laser beam.[3,4,6,15,16]

In order to perform future experiments with a prepared 2D system, repeatedly producing the 2D system with high stability is of key importance. This would ensure the high-fidelity manipulation of many-body quantum state and a sufficient signal-to-noise ratio (SNR) during imaging. A low fluctuation of the number of atoms favors the evaporative cooling to achieve lower temperatures for studying quantum phenomena. For example, a low temperature is critical to create unity filling Mott insulators[17,18] and to observe antiferromagnetic correlations[19,20] in optical lattices.

With this approach, the major challenges for preparing a 2D quantum gas are: Firstly, to provide a gradient magnetic field with low noises and slow drifts; Secondly, to compose a microwave pulse for coupling relevant atomic levels with high fidelity. Here we report on the techniques we developed to meet these demands. Briefly, based on the measured signal with a Hall sensor the current noise of the power supply

*Project supported by the National Key R&D Program of China (Grant No. 2016YFA0301603), the National Natural Science Foundation of China (Grant No. 11874341), Anhui Initiative in Quantum Information Technologies, and Chinese Academy of Sciences.

†Corresponding author. E-mail: yuanzs@ustc.edu.cn

© 2020 Chinese Physical Society and IOP Publishing Ltd

is suppressed by a fast feedback circuit and the current drift is corrected. The environmental magnetic field is monitored by a fluxgate type sensor and its drift is further compensated with a pair of Helmholtz coils whose current is delivered by an ultra-stable power supply. A microwave Landau–Zener transfer process is used to flip the internal state of atoms. The achieved efficiency, 99.92(3)%, of flipping atomic states indicates the performance of noise suppression. A repeated measurement on the spatial drift of the flipped atoms calibrates the drift of the magnetic field as 0.042(3) mG/hour, which outperforms the best results reported in a couple similar experiments.[16,21] In the following, we describe the experimental setup in Section 2. The overview on preparing the 2D quantum system is present in Section 3. The scheme on the applied magnetic field is given in Section 4. The methods on selecting one layer of the atoms by magnetic resonance are described in Section 5. The study on removing the atoms in other layers by a resonant laser beam is in Section 6. Noise reduction of the current supply is discussed in Section 7. Calibration of the method with microscopic imaging is provided in Section 8. Finally a short conclusion is presented in Section 9.

2. Setup

Our experimental setup is shown in Fig. 1. The pressure of the vacuum chamber (the volume in between the two glass viewports) is measured to be lower than 1.0×10^{-11} mbar, maintained by a non-evaporable getter pump. A Bose–Einstein condensate (BEC) of $4.0(3)\times10^6$ ^{87}Rb atoms in the state of $|F=1,m_F=-1\rangle$ is prepared in the center of the vacuum chamber via evaporative cooling in an cross dipole trap.

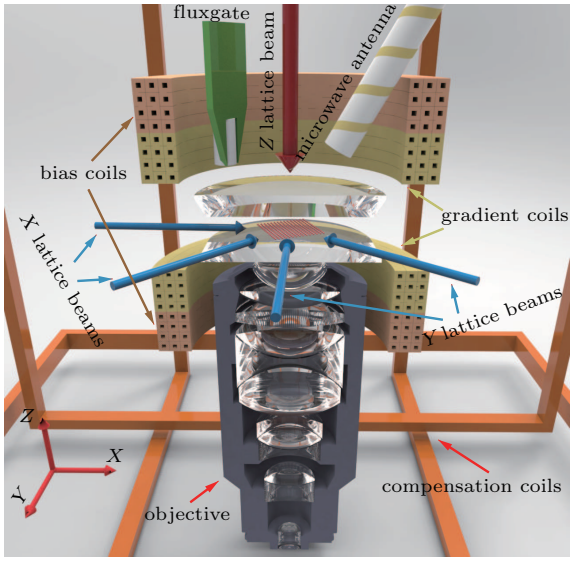


Fig. 1. Experimental setup. Parts of the compensation coils are shown, while the vacuum chamber made of stainless steel and the metal parts of the viewports are hidden. Each of X and Y lattices is formed by two laser beams of 532 nm crossed at an angle of 50°.

Beneath the chamber, a high-resolution objective situates with a numerical aperture of 0.8. The imaging resolution was calibrated to be 690 nm for the emitted light with a wavelength of 780 nm (^{87}Rb DII line). Meanwhile, the inner surface of the this viewport is coated with a high-reflective (HR) coating for the wavelength of 1064 nm. The incident laser beam of 1064 nm and its reflected beam from the inner surface together form the Z-lattice whose period is 532 nm. The X and Y lattices are both built by a pair of 532 nm laser beams crossed at the center with an angle of 50° resulting in a lattice constant of 630 nm. During fluorescence imaging, all the three lattices are raised to the maximal depth to pin the atoms on their own lattice sites.

After the BEC is achieved, the laser intensity of the Z-lattice is ramped up gradually and the atoms are loaded into a few layers of this lattice. Monolayer selection is performed with a Landau–Zener crossing (LZC) process,[22] which is implemented by a microwave knife. The gradient magnetic field is generated by two pairs of coils mounted outside the chamber. The microwave field is delivered by an antenna placed on top of the upper viewport for approaching the atoms as close as possible.

A single-axis fluxgate (FL-200, StefanMayer Instrument) with a bandwidth of 1 kHz and a range of ±2 G is placed about 3 cm away from the atoms to monitor the magnetic field along the Z direction. By adding three pairs of Helmholtz coils surrounding the chamber, we can generate bias fields along each direction to compensate for the stray magnetic field and adjust the direction of magnetic field gradient. The process will be described in detail in the following sections.

3. Overview on the method of preparing the 2D system

As mentioned above, the BEC atoms are loaded into a few layers of the Z-lattice by ramping up its trapping depth to $k_{\rm B}\times3.2$ μK corresponding to an axial trapping frequency of $2\pi\times24$ kHz. We use two states in the ground state $5^2S_{1/2}$ for the monolayer selection, i.e. $|F=1,m_F=-1\rangle$ and $|F=2,m_F=-2\rangle$, labeled by $|\downarrow\rangle$ and $|\uparrow\rangle$, respectively. Therefore, we also refer to the process of transferring between $|\downarrow\rangle$ and $|\uparrow\rangle$ as "spin flip". The gradient magnetic field is applied along the Z direction. Therefore, the Zeeman energy splitting of the atoms becomes spatially dependent.

To select one layer of the atoms in the Z-lattice, we take the following steps sequentially. First, all the atoms originally prepared in $|\downarrow\rangle$ are transferred to $|\uparrow\rangle$ with a global microwave sweep, an LZC pulse explained later in Section 5. Then, once all the atoms are in $|\uparrow\rangle$, a single layer of atoms are transferred back to $|\downarrow\rangle$ by a second LZC pulse with a narrower sweeping range. Finally, with a laser beam resonantly coupling to the transition $|5^2S_{1/2},F=2\rangle\rightarrow|5^2P_{3/2},F=3\rangle$, we push all the atoms in $|\uparrow\rangle$ out and leave this single layer of atoms in $|\downarrow\rangle$. To achieve a high precision and stability of these operations, several technical issues will be addressed in the future sections.

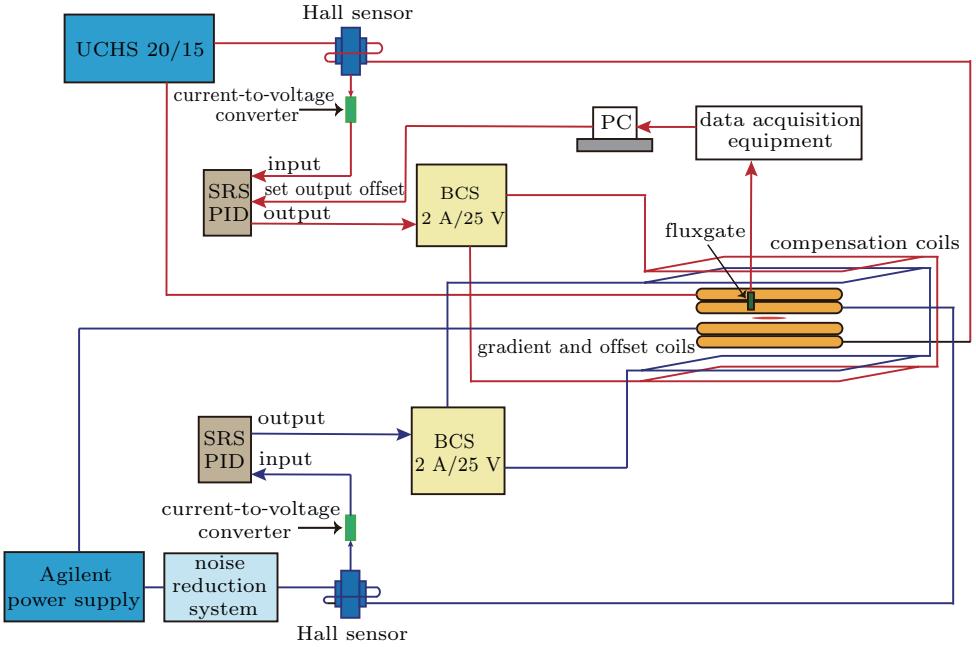


Fig. 2. Current supplies and the coils for providing a stabilized low-noise magnetic field. The commercial proportional–integral–derivative (PID) units (SRS, SIM960) control the output of BCS current sources to actively compensate the current drift of coils, while its output offset is modified every experimental trial to correct environmental magnetic field drift.

4. Scheme on the magnetic fields

To perform spin flip for the atoms in one particular layer while leaving the rest unchanged, it is necessary to create spatially dependent energy splitting along the Z axis with a gradient magnetic field. Two points should be considered carefully. One is that the magnetic field gradient should be strong enough to make the energy splitting of atoms in neighboring layers highly distinguished by the second microwave pulse. The other one is that the magnetic field in the target layer should be homogeneous for a high-fidelity spin-flip of all the atoms. Write the gradient as

$$\nabla|\boldsymbol{B}_{\text{total}}| = \frac{\partial|\boldsymbol{B}_{\text{total}}|}{\partial x}\boldsymbol{e}_x + \frac{\partial|\boldsymbol{B}_{\text{total}}|}{\partial y}\boldsymbol{e}_y + \frac{\partial|\boldsymbol{B}_{\text{total}}|}{\partial z}\boldsymbol{e}_z, \quad (1)$$

where $\boldsymbol{e}_x$, $\boldsymbol{e}_y$ and $\boldsymbol{e}_z$ are unit vectors along X, Y and Z directions, these constrains define the following relationship in the target layer

$$\frac{\partial|\boldsymbol{B}_{\text{total}}|}{\partial z} \gg \frac{\partial|\boldsymbol{B}_{\text{total}}|}{\partial x} \simeq \frac{\partial|\boldsymbol{B}_{\text{total}}|}{\partial y} \approx 0. \quad (2)$$

To satisfy the above condition, we first place a pair of anti-Helmholtz coils (labeled gradient coils in Fig. 1) to generate a quadrupole field which creates the gradient. However, solely with these coils, the generated magnetic field in the X–Y plane is too steep and a high-fidelity spin-flip can not be achieved for all the atoms simultaneously in the target layer. Therefore, a second pair of Helmholtz coils (labeled bias coils in Fig. 1) are necessary to create a strong offset magnetic field to shift the gradient center of the above field. Then the field gradient in the X–Y plan is reduced dramatically within the region of the target layer. Suppose that the center of gradient coils is origin of coordinates,we model the above configuration of coils as follows:

$$\boldsymbol{B}_{\text{total}} = k_x x\boldsymbol{e}_x + k_y y\boldsymbol{e}_y + (k_z z + B_0)\boldsymbol{e}_z, \quad (3)$$

$$|\boldsymbol{B}_{\text{total}}| = \sqrt{(k_x x)^2 + (k_y y)^2 + (B_0 + k_z z)^2}, \quad (4)$$

k_x, k_y, k_z are the quadrupole field's gradients along each direction near the center. As magnetic fields are source-free, $k_x = k_y = k_z/2$. $B_0\boldsymbol{e}_z$ is the offset field generated by the Helmholtz coils. Therefore, we can calculate different components in magnetic field gradient as

$$\frac{\partial|\boldsymbol{B}_{\text{total}}|}{\partial x} = \frac{2k_x^2 x}{\sqrt{(k_x x)^2 + (k_y y)^2 + (B_0 + k_z z)^2}} = \frac{2k_x^2 x}{|\boldsymbol{B}_{\text{total}}|}, \quad (5)$$

$$\frac{\partial|\boldsymbol{B}_{\text{total}}|}{\partial y} = \frac{2k_y^2 y}{\sqrt{(k_x x)^2 + (k_y y)^2 + (B_0 + k_z z)^2}} = \frac{2k_y^2 y}{|\boldsymbol{B}_{\text{total}}|}, \quad (6)$$

$$\frac{\partial|\boldsymbol{B}_{\text{total}}|}{\partial z} = \frac{2k_z(B_0 + k_z z)}{\sqrt{(k_x x)^2 + (k_y y)^2 + (B_0 + k_z z)^2}} = \frac{2k_z(B_0 + k_z z)}{|\boldsymbol{B}_{\text{total}}|}. \quad (7)$$

As can be seen in Eq. (4), increasing B_0 provides a larger $\boldsymbol{B}_{\text{total}}$, therefore reduces the components along X and Y directions (Eqs. (5) and (6)) in the magnetic field gradient. Thus, when we generate a B_0 strong enough, the magnetic field in the X–Y plane is flattened while the gradient component along Z direction changes very little near the Z axis.

In total, we generate a magnetic field gradient of 100 G/cm combined with an offset magnetic field of 35 G at Z direction. Ideally, atoms should be prepared close to the center of the gradient coils at which gradient coils create zero magnetic field, so that the current noise of power supply can only bring little magnetic noise to atoms. However, the focus of the high-resolution objective, where the target layer should be located, was aligned 1 mm below the gradient center due to assembly deviation. Then, the total field strength at the position of the target layer is $|\boldsymbol{B}_{\text{total}}| = 0.1\ \text{cm} \times 100\ \text{G/cm} + 35\ \text{G} = 45\ \text{G}$, proportional to the current of the power supplies. Thus, the atoms suffer directly from the current noises arising from the relevant power supplies.

The radius of the atom cloud in our experiment is smaller than 50 μm. In this region, we realize a very flat magnetic field in the X–Y plane as $|\boldsymbol{B}_{\text{total}}(50\ \mu\text{m})| - |\boldsymbol{B}_{\text{total}}(0)| < 0.7$ mG. Meanwhile, the lattice constant in the Z direction, 532 nm, results in a $\Delta B = 5.32$ mG (equivalent to a Zeeman shift of $2.1 \times 5.32 = 11.17$ kHz) difference between the neighboring layers. Therefore, equation (2) is satisfied. In principle, a magnetic field composed of a gradient field and an offset can be generated by a single coil. However, our method which combines anti-Helmholtz coils and Helmholtz coils provides the degree of freedom to modify the ratio of magnetic field gradient to field strength.

As the strong magnetic fields require large electric currents which cause dramatically heating to the coils, water cooling is employed to stabilize the temperature of these coils. Suppressing the temperature fluctuation of the coils is of great importance for two aspects: Firstly, the thermal deformation of the coils is reduced, which results in a precisely stable magnetic field around the target layer of atoms. Secondly, the thermal disturbance to the surrounding air is reduced, which results in a stable refractive index favorable for stabilizing the beam paths. Here the coils are made of hollow copper wires with the central hole radius of 1.25 mm for injecting temperature actuated water. Meanwhile, the temperatures of the coils are monitored by sensors (Texas Instruments, LM35DZ) as reference to prevent overheating.

5. Selecting one layer of atoms by magnetic resonance

Transferring ^{87}Rb atoms between $|\downarrow\rangle$ and $|\uparrow\rangle$ can be performed either by Rabi π pulses[23] or the adiabatic LZC.[22] However, the former is more sensitive to magnetic noises since the phase and amplitude of Rabi oscillations could be modified by the magnetic fluctuations by changing the detunings. In contrast, the latter has a much higher tolerance to magnetic noises. Therefore, we employ the LZC in our experiment for flipping the atomic sates.

The Zeeman splitting of $|\uparrow\rangle$ and $|\downarrow\rangle$ is 2.1 kHz/mG and the magnetic field gradient induces an energy difference of 11.17 kHz between neighboring layers. Thus, we perform a microwave LZC by sweeping its frequency from -4 kHz to 4 kHz with respect to the resonant frequency.

The time dependence of the microwave frequency and strength is of key importance for the transfer efficiency. To achieve a high efficiency, we use a hyperbolic secant (HS1) pulse[24] whose Rabi frequency $\Omega(t)$ and frequency detuning $\Delta(t)$ are defined as follows:

$$\Omega(t) = \Omega_{\max}\text{sech}\left[\beta\left(\frac{2t}{T} - 1\right)\right], \tag{8a}$$

$$\Delta(t) = \frac{\Delta_{\text{range}}}{2}\tanh\left[\beta\left(\frac{2t}{T} - 1\right)\right]. \tag{8b}$$

Here $\Omega_{\max}$ is the maximum Rabi frequency, T is the pulse duration, Δ_{range} is the frequency range set to 8 kHz, and β is the cut-off factor set to 5. These values are optimized according to our experimental conditions.

Figure 3 illustrates the reason of using an HS1 pulse for flipping the atoms. A theoretical estimation of the transfer efficiency shows that the HS1 pulse produces a flat-top profile with the efficiency close to 1 as long as the resonant frequency is within the sweeping range, and falls sharply to nearly zero once the resonant frequency lies outside the sweeping range. This feature is particularly useful for flipping the target layer completely while preventing the atoms in the neighboring layers from being disturbed in case a moderate magnetic fluctuation is present. In contrast, a similar microwave pulse with a chirped modulation produces an undesiredly oscillating efficiency curve.

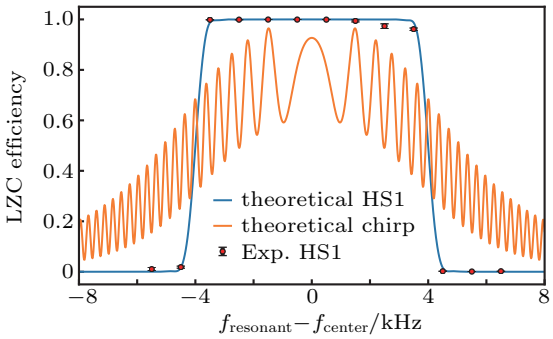


Fig. 3. Comparison between the estimated LZC efficiencies and the measured results. Theoretical estimations with a chirped sweep (orange curve) and HS1 pulse (blue curve). Both the sweeps have the same range of ±4 kHz around the central frequency and same pulse duration of 4 ms. For the HS1 pulse, $\Omega_{\max}$ is set to 3.21 kHz. In chirped modulation, the Rabi frequency is fixed at $\Omega_{\max}$, while the microwave frequency changes with time linearly. The experimental results match very well with the theoretical estimation.

In our experiment, we measured the transfer efficiency when applying the HS1 pulse to a cloud of BEC atoms in a homogeneous magnetic field of 1 G along the Z direction. All the atoms N_0 in $|\downarrow\rangle$ are first transferred to $|\uparrow\rangle$ by a microwave

LZC pulse and subsequently back to $|\downarrow\rangle$ by a second identical pulse. Then the number of atoms in $|\uparrow\rangle$ is measured as $N_{|\uparrow\rangle}$. With the knowledge of N_0 and $N_{|\uparrow\rangle}$, we can derive the transfer efficiency η given the following relations

$$2\eta(1-\eta) = \frac{N_{|\uparrow\rangle}}{N_0}, \tag{9}$$

resulting in

$$\eta_{\pm} = \frac{1}{2}\left(1 \pm \sqrt{1-2\frac{N_{|\uparrow\rangle}}{N_0}}\right). \tag{10}$$

To determine the sign in the expression of $\eta_{\pm}$, we measure the number of spin-up atoms after applying the first LZC pulse. When the measured number is larger than $N_0/2$, we choose $+$. Otherwise, we choose $-$. Shown in Fig. 3, our measured efficiency of the LZC process shows a good agreement with the relevant theoretical estimations. This is an evidence that the environmental magnetic noises are well suppressed in our system.

The Rabi frequency of the pulse is proportional to the square root of the microwave power. Measuring the Rabi oscillation of the atoms under a microwave power of 2 dBm delivered by the signal generator, we calibrate the Rabi frequency as 3.21(2) kHz. Under the magnetic field with a gradient of 100 G/cm, we set a sweep range of $\pm$800 kHz, a pulse length of 20 ms, and a Rabi frequency of 14 kHz to flip the atoms in all layers. This is called a global flip. In contrast, a range of $\pm$4 kHz, a pulse length of 4 ms and a Rabi frequency of 3.21 kHz are employed to flip a single layer of interest. This is called a single flip. Its efficiency is measured to be 99.92(3)%.

In principle, a shorter HS1 pulse with a higher Rabi frequency and a reduced sweep range could also be used without decreasing the efficiency under the condition of on resonance. However, with such a pulse, the two edges of the efficiency curve in Fig. 3 will be less sharp, leading to a smaller flat region of the curve in the middle of the sweep range. Therefore, for a same drift of the environmental magnetic field, the long-term stability of the efficiency gets worse compared with the one in the present experiment.

6. Removing atoms in other layers with a resonant laser pulse

In our experiment, a typical spin-flip efficiency reaches over 99%. However, there are still about hundred atoms remained in their initial state $|\downarrow\rangle$ after a global flip over more than 10^5 atoms. These atoms will create noises during final detection by fluorescence imaging. Hence, we use a σ^- polarized repump laser resonant with $|\downarrow\rangle \rightarrow |5^2\mathrm{P}_{3/2}, F=2\rangle$ to transfer them to $|\uparrow\rangle$ via a spontaneous Raman transition $|\downarrow\rangle \rightarrow |5^2\mathrm{P}_{3/2}, F=2\rangle \rightarrow |\uparrow\rangle$.

After the single flip pulse, only atoms in the target layer are transferred back to $|\downarrow\rangle$, while the rest in other layers still remain in $|\uparrow\rangle$. They are removed with a σ^- laser, the push-out laser, resonant with the circling transition $|\uparrow\rangle \leftrightarrow |5^2\mathrm{P}_{3/2}, F=3\rangle$. Therefore, no dark state involves in this process resulting in a removal efficiency $> 99\%$.

7. Noise reduction and stabilization of the magnetic field around the atoms

Intuitively, the single-layer selection requires the noise and drift of the magnetic field to be much lower than ΔB. A numerical simulation on the LZC process shows that the magnetic fluctuation should be lower than 1 mG for maintaining a spin-flip efficiency over 99%. Since the magnetic field around the atoms is about 45 G, this corresponds to a noise level of 22 ppm. In principle, it is straightforward to detect the magnetic field with a sensor and then stabilize the field strength to a certain value by an active feedback circuit.[25–27] In our experiment, however, the magnetic field is too strong ($\sim$ 45 G) that no available sensor provides a proper precision at such a strength. To satisfy this stringent request, we employ three approaches: (a) Suppress the electronic noise of the current supply with a fast feedback circuit. (b) Compensate for the drift of the magnetic field induced by the drift of current supply. (c) Compensate for the drift of environmental magnetic field.

7.1. Noise reduction of the current supply

The offset coils and the gradient coils create magnetic fields at the position of atoms with the factors of 1.75 G/A and 0.1 G/A, respectively (see Fig. 2). It is important to suppress the magnetic noises generated by both coils. In our setup, an ultralow-noise commercial current supply (HighFinesse UHCS20/15) is used to power the offset coils. Its rms noise is 0.2 mA at the working current of 20 A. The current of the gradient coils is delivered by a commercial power supply (Agilent 6682 A), whose rms current noise is measured to be 5.5 mA at the current of 100 A.

We designed a noise reduction system with an insulated-gate bipolar transistor (IGBT) and a Hall sensor (LEM, ITN 600-S). The power supply, gradient coils and the IGBT are connected in series. The Hall sensor detects the current in coils and delivers a scaled current. This signal is then transformed into a voltage with a sampling resistor which has an extremely low temperature coefficient of 0.5 ppm/K. Afterwards, this voltage is fed into a PID electronic board which provides the driving signal for the gate of IGBT.

The rms noise is suppressed to 0.6 mA at the working current of 100 A as shown in Fig. 4. From the noise spectrum in Fig. 4(b), we can see that the noise reduction system has a bandwidth larger than 1 kHz. Particularly, a noise reduction

of 20 dB is observed at 50 Hz. The rms noises are measured by a Hall sensor (LEM, ITN 600-S) and a digital multimeter (Agilent 34410) with a sampling rate of 10000 samples/s. Thanks to the noise reduction approach, the total rms magnetic noise induced by the noise of power supplies is estimated to be 0.36 mG.

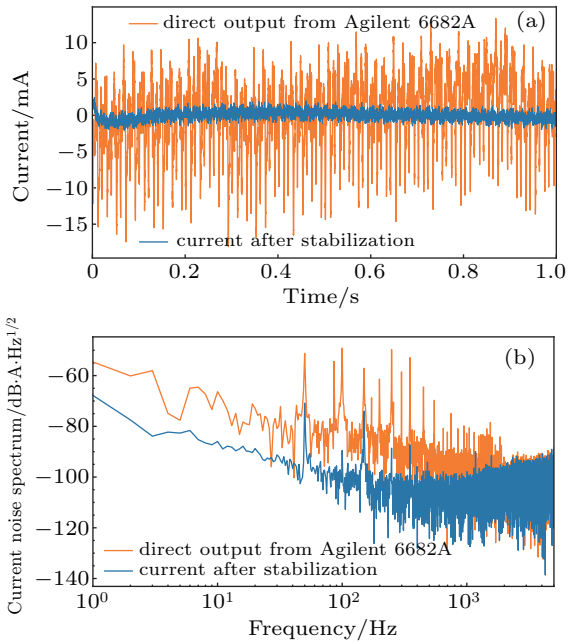


Fig. 4. Comparison of the direct output from the current supply and the output from the noise reduction circuit. Current fluctuation in time domain, in which the mean value is subtracted from the original data. Current noise spectrum.

7.2. Compensation of the magnetic field fluctuation induced by the current drift

The long-term drift of current is destructive for the repeatability of selecting the same single layer of atoms. Though the above noise reduction circuit has a bandwidth covering low frequencies, we still observe an obvious drift of the current running in either the offset coils or the gradient coils per other Hall sensors (LEM, ITN 600-S). Based on the measured value of current in the offset coils, the induced drift of the magnetic field is actively compensated by a pair of Helmholtz coils (C1) made of one winding of wire. The C1 coils generate a bias field with the factor of 50 mG/A and are powered by an analog-controlled current supply (HighFinesse BCS 2 A/25 V). One easily finds that a current of 35 mA in C1 compensates the drift of magnetic field induced by the current drift of 1 mA in the offset coils. This scheme offers a fine compensation. Therefore, it is used as well for compensating the drift of current in the gradient coils.

7.3. Compensation of the drift of the environmental magnetic field

The noise and drift of the current in the magnetic coils are suppressed with the above two approaches. Finally, the drift of the environmental magnetic field should be considered.

Measuring the Rabi oscillation between two hyperfine levels of the atoms shows that the noise of the environmental magnetic field along the Z direction is around 0.4 mG, which agrees with the measurement by a fluxgate-type sensor. Therefore the noise of the environmental magnetic field has a negligible impact on the efficiency of single-layer selection. However, the slow drift of the environmental magnetic field is on the level of a few mG and has a larger impact. Thus, we implement a static compensation approach. Before each experimental trial, we turn off the currents in all coils and measure the background magnetic field for 1 s with a fluxgate sensor. The measured value is acquired by a computer, then an appropriate current will be calculated and fed into the compensation coil of C1 with the help of the real-time control system. This process is carried out automatically in every experimental trail.

Based on the above three approaches, both the noise and drift of the magnetic field around the atoms are suppressed. The performance of the whole solution is characterized by directly testing the response of the atoms.

8. Calibration of the method by microscopic imaging

Ideally, the magnetic field gradient should be well aligned along the Z direction and orthogonal to the plane of each layers. However, in the experiment, the tilt of the coils as well as a background magnetic field may change the direction of the magnetic field gradient, resulting in a misalignment. Suppose a background magnetic field along the X direction ($\boldsymbol{B} = B\boldsymbol{e}_x$), an angle θ will be created between the direction of gradient and the Z axis as

$$\begin{aligned}\tan(\theta) &\sim \frac{\partial \mid \boldsymbol{B}_{\text{total}} \mid /\partial x}{\partial \mid \boldsymbol{B}_{\text{total}} \mid /\partial z} \sim \frac{k_x(k_x r + B)}{k_z(k_z z + B_0)} \\ &\sim \frac{k_x x + B}{2(k_z z + B_0)} \sim \frac{B}{2B_0}.\end{aligned} \tag{11}$$

The last term corresponds to the approximation for $x, z \to 0$. The direction of magnetic field gradient is not orthogonal to the planes of atom layers. Thus a single-frequency microwave field may be resonant with a few layers. The microwave knife will cut across several layers and stripes will be seen during *in situ* imaging with the microscope described above. Though this misalignment is not desirable in our experiment and will be corrected carefully, we would intentionally create this misalignment and take the visible fringes as observables for calibrating the system (see Fig. 5). The reason is that noises of the magnetic fields will blur the fringes while drift of the magnetic fields causes moving of the fringes.

As shown in Fig. 5, we applied an offset magnetic field on the X–Y plane using the compensation coils to tilt the gradient. Before the noises of the magnetic fields are suppressed, we only observe blurred fringes as in Fig. 5(a), indicating a

low LZC efficiency. In contrast, the fringes get clear when we implement the noise reduction system, showing a high LZC efficiency.

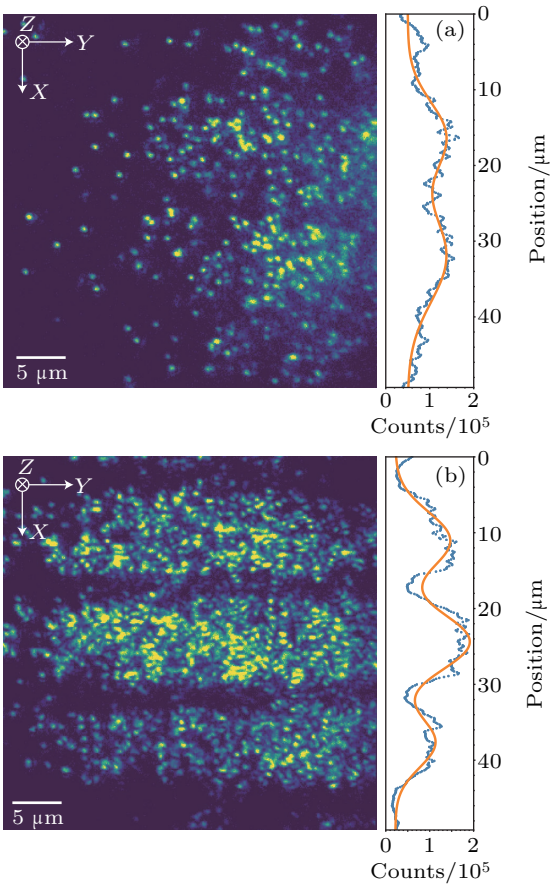


Fig. 5. *In situ* imaging of the atoms selected from a few layers of the 1D optical lattice. (a) Blurred fringes due to the noises of magnetic field before applying the noise reduction system. (b) The fringes get much clear after the noise reduction system is optimized.

In order to study the drift of magnetic field around the atoms, we run the above experiment repeatedly to monitor the drift of fringes. An 8-hour measurement was performed, as shown in Fig. 6. The period, 12.4(4) μm, of the fringes indicates a tilt angle of $\theta = 2.46(8)^\circ$. The rms width of the curve in Fig. 6 shows a short-term drift of the magnetic field within the range of 0.23 mG. Meanwhile, by fitting the data of fringe 2 with a linear function, a clear long-term drift (in red, lower panel) with an average drift speed of 0.042(3) mG/hour is obtained. The sweep range of the HS1 pulse for selecting one layer is ±4 kHz, corresponding to a range of magnetic field of ±1.9 mG. Therefore, preparing the 2D single layer of atoms can be continuously carried out with a high efficiency for 48 hours before the resonant condition is gone. This means that we only need to re-adjust the frequency center once a day.

Besides the three approaches introduced in Section 7, we find that the stability of the generated magnetic field suffers from the temperature fluctuation of the coils due to thermal deformations which should be suppressed as well. Figure 6(b) shows the two measurements on the phase of the fringes at different temperature fluctuations. The orange data points were taken when there was a temperature oscillation with an amplitude of ±0.7 K. A period of 3.3 min is observed in the drift of the strength of magnetic field, which matches the temperature change of the coils and of the cooling water delivered by the chiller. To minimize this effect, we employed a better water chiller for coils and the temperature fluctuation was decreased to ±0.1 K. As a result, the oscillation amplitude of the magnetic field is reduced from ±0.75 mG to ±0.25 mG (blue data points).

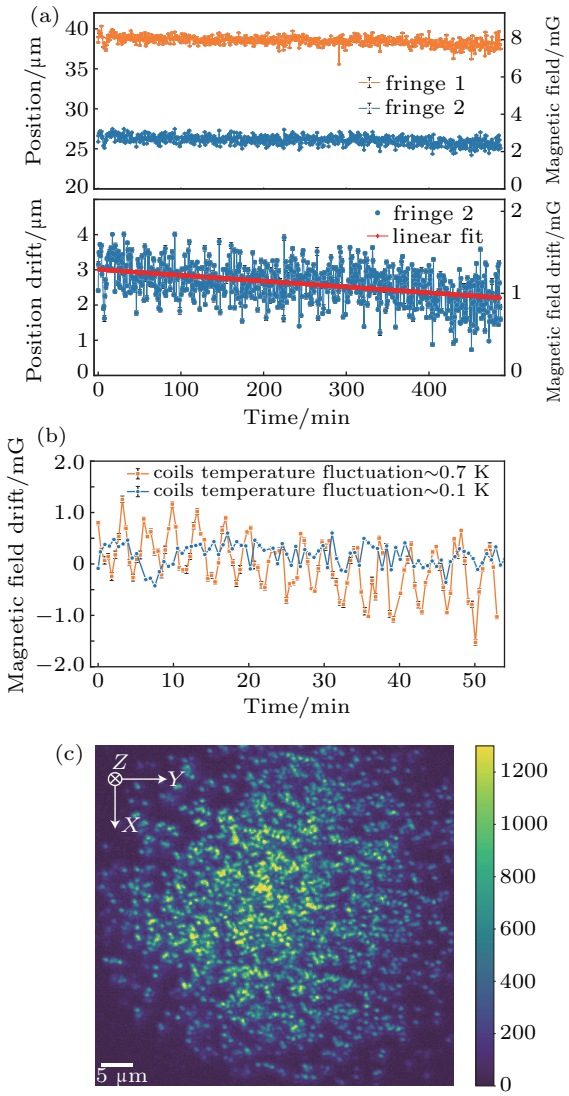


Fig. 6. Characterization of the drift of magnetic field. (a) Drift of center of the stripes indicates the drift of magnetic field. (b) Drift of the magnetic field under different temperature fluctuations of the coils. To obtain the center of stripes, we integrates the counts in each row to get the curve and then fits it with a sum of gaussian functions to get the position of peaks, as shown in right panels of Fig. 5. The error bars show 1σ statistical uncertainty of the fitted centers. The relationship between the drift of stripes and the drift of magnetic fields is estimated with the magnetic field gradient and the structure of stripes. (c) An exemplary image of the atoms selected in a single layer when the noise and drift of the magnetic fields are suppressed.

It is worth mentioning that some groups synchronize their experimental sequence to the AC line phase to reduce the influence of 50 Hz noise.[21,28] However, according to our test, it is unnecessary to do so since the above approaches suppress such

a noise effectively. After the misalignment of magnetic field gradient is corrected, we always achieve an efficiency higher than 99% for preparing the single layer which does not depend on the synchronization. Figure 6(c) shows an exemplary image of the atoms selected in a single layer shoot with the microscope when the noise and drift of the magnetic fields are suppressed.

9. Conclusion

We have developed a technique on preparing a 2D quantum gas based on slicing a single layer of atoms trapped in a few layers of pancake-shaped optical traps. To achieve a high efficiency for this preparation, a Landau–Zener-cross microwave pulse with well-designed profile is applied to improve the noise tolerance and stability. The rms noise of magnetic field induced by the current supplies is reduced to 0.36 mG with a home-built noise reduction system. The slow drift of magnetic field is minimized with a static compensation circuit and a more stable water chiller. The effectiveness of these approaches was verified by observing the response of atoms with *in situ* microscopic imaging. Finally a slow drift speed of 0.042(3) mG/hour is achieved, promising a continuous experiment of 48 hours for maintaining the preparation efficiency of the 2D quantum gas as 99.92(3)%. Synchronizing the experimental sequence to the phase of the AC line is found to be unnecessary for achieving the high efficiency.

Our work can be extended to the creation of a bilayer lattice system, in which disentangling two layers to create a low-entropy single layer system is proposed.[29] Meanwhile, the home-made ultrastable current supply and the full scheme of stabilizing magnetic fields have promising applications in both scientific researches and various industries.

References

[1] Bloch I, Dalibard J and Zwerger W 2008 *Rev. Mod. Phys.* **80** 885
[2] Bakr W S, Gillen J I, Peng A, Fölling S and Greiner M 2009 *Nature* **462** 74
[3] Sherson J F, Weitenberg C, Endres M, Cheneau M, Bloch I and Kuhr S 2010 *Nature* **467** 68
[4] Haller E, Hudson J, Kelly A, Cotta D A, Peaudecerf B, Bruce G D and Kuhr S 2015 *Nat. Phys.* **11** 738
[5] Cheuk L W, Nichols M A, Okan M, Gersdorf T, Ramasesh V V, Bakr W S, Lompe T and Zwierlein M W 2015 *Phys. Rev. Lett.* **114** 193001
[6] Edge G J A, Anderson R, Jervis D, McKay D C, Day R, Trotzky S and Thywissen J H 2015 *Phys. Rev. A* **92** 063406
[7] Parsons M F, Huber F, Mazurenko A, Chiu C S, Setiawan W, Wooley-Brown K, Blatt S and Greiner M 2015 *Phys. Rev. Lett.* **114** 213002
[8] Islam R, Ma R, Preiss P M, Eric Tai M, Lukin A, Rispoli M and Greiner M 2015 *Nature* **528** 77
[9] Choi J y, Hild S, Zeiher J, Schauß P, Rubio-Abadal A, Yefsah T, Khemani V, Huse D A, Bloch I and Gross C 2016 *Science* **352** 1547
[10] Kosterlitz J M and Thouless D J 1973 *J. Phys. C: Solid State Phys.* **6** 1181
[11] Berezinskii V L 1972 *J. Exp. Theor. Phys.* **34** 610
[12] Dai H N, Yang B, Reingruber A, Xu X F, Jiang X, Chen Y A, Yuan Z S and Pan J W 2016 *Nat. Phys.* **12** 783
[13] Gillen J I, Bakr W S, Peng A, Unterwaditzer P, Fölling S and Greiner M 2009 *Phys. Rev. A* **80** 021602
[14] Bender H, Courteille P, Zimmermann C and Slama S 2009 *Appl. Phys. B: Lasers Opt.* **96** 275
[15] Karski M, Förster L, Choi J M, Steffen A, Belmechri N, Alt W, Meschede D and Widera A 2010 *New J. Phys.* **12** 065027
[16] Peaudecerf B, Andia M, Brown M, Haller E and Kuhr S 2019 *New J. Phys.* **21** 013020
[17] Greif D, Parsons M F, Mazurenko A, Chiu C S, Blatt S, Huber F, Ji G and Greiner M 2016 *Science* **351** 953
[18] Cheuk L W, Nichols M A, Lawrence K R, Okan M, Zhang H and Zwierlein M W 2016 *Phys. Rev. Lett.* **116** 235301
[19] Mazurenko A, Chiu C S, Ji G, Parsons M F, Kanász-Nagy M, Schmidt R, Grusdt F, Demler E, Greif D and Greiner M 2017 *Nature* **545** 462
[20] Boll M, Hilker T A, Salomon G, Omran A, Nespolo J, Pollet L, Bloch I and Gross C 2016 *Science* **353** 1257
[21] Edge G 2017 *Imaging Fermionic Atoms in a Quantum Gas Microscope* (PhD dissertation) (Toronto: University of Toronto)
[22] Zener C 1932 *Proc. R. Soc. Lond. A* **137** 696
[23] Foot C J 2005 *Atomic Physics* (New York: Oxford University Press) pp. 127–128
[24] Garwood M and DelaBarre L 2001 *J. Magn. Reson.* **153** 155
[25] Dedman C J, Dall R G, Byron L J and Truscott A G 2007 *Rev. Sci. Instrum.* **78** 024703
[26] Merkel B, Thirumalai K, Tarlton J E, Schäfer V M, Ballance C J, Harty T P and Lucas D M 2019 *Rev. Sci. Instrum.* **90** 044702
[27] Xu X T, Wang Z Y, Jiao R H, Yi C R, Sun W and Chen S 2019 *Rev. Sci. Instrum.* **90** 054708
[28] Elíasson O, Heck R, Laustsen J S, Napolitano M, Müller R, Bason M G, Arlt J J and Sherson J F 2019 *J. Phys. B: At. Mol. Opt. Phys.* **52** 075003
[29] Kantian A, Langer S and Daley A J 2018 *Phys. Rev. Lett.* **120** 60401